CFD Analysis of the HyShot Supersonic Combustion Flight Experiment Configuration

Sebastian Karl* and Klaus Hannemann.†
German Aerospace Center, DLR, Institute of Aerodynamics and Flow Technology, 37073 Goettingen, Germany

Johan Steelant‡ and Andreas Mack.§
European Space Research and Technology Center, ESTEC, 2200 AG Noordwijk, The Netherlands

Testing of the HyShot II scramjet configuration was carried out in the High Enthalpy Shock Tunnel Goettingen, HEG, of the German Aerospace Center, DLR. Computational fluid dynamics (CFD) is applied to support the analysis of experimental results and for the prediction of the free stream conditions in the HEG test section. Numerical simulations of the flow in the complete HyShot configuration for fuel on and off conditions were performed. This paper describes the laminar and turbulent modeling approaches for the CFD analysis and presents numerical results of both the HEG nozzle flow and the turbulent reacting flow in the Hyshot scramjet configuration. Numerical results are compared to the experiment.

I. Introduction

To reduce the traveling time of long-distance flights, e.g. Brussels to Sydney, in about 2 to 4 hours, advanced propulsion concepts and technologies need to be developed for flight regimes with Mach numbers ranging from 4 to 8. One possible technology to achieve this goal is the Supersonic Combustion Ramjet (scramjet) engine.

The subject of the LAPCAT[1] project of the 6th European Framework Program is the development of key technologies for advanced high speed air-breathing propulsion systems. The work that is presented in this paper is related to the scramjet research activities in the LAPCAT project. The main focus is on the numerical investigation of the turbulent reacting flow inside the HyShot[2] Mach 8 scramjet configuration.

Although significant advances have been made in developing scramjet engines, including the University of Queensland's supersonic combustion flight experiment HyShot and the flight of NASA's X-43 in March 2004, major scientific and technological challenges remain. The kinetic energy of the free stream air entering the engine is of the same order of magnitude as the potential combustion heat release. This results in small net thrust coefficients at high flight velocities. Thus, minimizing the aerodynamic drag of scramjet engines becomes as important for vehicle performance as maximizing the thrust. Due to the complexity of the flows in the propulsion systems of advanced hypersonic transport vehicles, a strong link of ground based experiments, flight testing and computational fluid dynamics is needed to improve the understanding of flow phenomena such as fuel mixing, ignition delay, influence of blunt leading edges and boundary layer bleeds.

Experimental investigations of the HyShot scramjet flight test configuration utilizing a 1:1 scale were carried out in the High Enthalpy Shock Tunnel Goettingen, HEG. The results of the test campaigns in HEG show qualitative agreement with the flight data and confirm the establishment of supersonic combustion. The experimental setup, applied measurement techniques and results were described in detail by Gardner et al.[3].

The DLR unstructured/hybrid flow solver TAU[4] was extended for the modeling of the flow path in supersonic combustion ramjet engines. Appropriate models for turbulent hydrogen combustion were implemented. TAU was used to determine the free stream conditions in the HEG test section, to simulate the HyShot intake flow field and for the numerical investigation of the turbulent reacting flow in the combustor. The results presented in this paper correspond to the HEG condition XII which duplicates the HyShot free stream conditions at a flight altitude of 32.5 km. Results obtained at a lower flight altitude of 28 km were previously investigated by Steelant et al.[5].

* Research Scientist, Spacecraft Section, Sebastian.Karl@dlr.de, AIAA member
† Head of Spacecraft Section, Klaus.Hannemann@dlr.de, AIAA member
‡ Research Scientist, Johan.Steelant@esa.int, AIAA member
§ Internal Research Fellow, Andreas.Mack@esa.int, AIAA member

II. Numerical Model

All numerical investigations within this study were performed with the hybrid structured/unstructured DLR-Navier-Stokes solver TAU[4], which is validated for a wide range of steady and unsteady sub-, trans- and hypersonic flow cases[6]. The TAU-code is a second order finite-volume flow solver for the Euler and Navier-Stokes equations in the integral form using Eddy-Viscosity and Reynolds-Stress models or Detached Eddy Simulation for turbulence modeling. For the present investigations, the Reynolds averaged Navier Stokes equations (RANS) applying the one-equation Spalart-Allmaras[7] and the two-equation Wilcox k-ω[8] turbulence models were solved. The AUSMDV[9] flux vector splitting scheme is applied together with MUSCL gradient reconstruction to achieve second order spatial accuracy.

Different detailed finite rate chemistry models for hydrogen / air combustion were implemented in the TAU code within the LAPCAT project. These are based on previous extensions for chemical and thermal non-equilibrium flows in high enthalpy aerothermodynamics[10].

The flow is considered to be a reacting mixture of thermally perfect gases. A transport equation is solved for each individual species. The chemical source term in this set of transport equations is computed from the law of mass action by summation over all participating reactions. The forward reaction rate is computed from the modified Arrhenius law and the backward rate is obtained from the equilibrium constant which is computed directly from the partition functions of the participating species. The thermodynamic properties (energy, entropy, specific heat) are calculated from the partition functions for each individual species in the reacting gas mixture. The advantage of this approach is its high flexibility. Extensions such as multi temperature models to handle thermal non-equilibrium effects are easily possible. Knowing the mixture composition and the thermodynamic state of the individual species the properties of the reacting gas mixture are computed using suitable mixture rules such as proposed by Wilke[11] for the viscosity and by Herning and Zipperer[12] for the heat conductivity.

A fully catalytic wall boundary condition was used, i.e., a Dirichlet boundary condition for the species mass fractions is set according to the local equilibrium composition.

The species diffusion fluxes are modeled using Fick's law applying an averaged diffusion coefficient for all species This approximate diffusion coefficient is computed using the viscosity and a constant Schmidt number of $Sc = 0.7$. For turbulent flows the viscosity is taken to be the sum of the laminar and the turbulent contributions. The turbulent viscosity is then derived from the applied turbulence model (e.g. computed from turbulent kinetic energy and length scale for the application of the k-ω model or directly obtained from the Spalart-Allmaras model).

Thermal non-equilibrium flows are computed by solving an additional transport equation for the vibrational energy of each molecule in non-equilibrium. The relaxation of vibrational energy is modeled according to the Landau-Teller[13] approach and the vibrational relexation times are obtained from the correlation of Millikan and White[14].

An assumed Probability-Density-Function (PDF) model as described by Gerlinger[15] was implemented in the DLR-Tau Code to model the influence of turbulent fluctuations on the species source terms from detailed chemistry schemes. The major advantages of this approach are,

- no limitations concerning premixed, non-premixed or partially premixed combustion,
- no limitations concerning the range of Damköhler numbers,
- successful application to supersonic combustion problems has already been demonstrated[15,16], and
- straightforward implementation in a chemical non-equilibrium code, highly robust and numerically efficient.

The averaged turbulent chemical source terms are computed by integrating the laminar expression over all realizable temperatures and species concentrations which are weighted by the probability of their occurrence.

These probabilities are given by presumed shape PDFs (Gaussian distribution for the temperature and multi-variate beta distributions for the species concentrations). Statistical independence of temperature and species concentration fluctuations are assumed. Two additional transport equations for the variance of temperature and the sum of the variances of species concentrations are solved to completely describe the PDF at each point of the flow field.

III. Nozzle Flow and Determination of the Free Stream Conditions in the HEG Test Section

The evaluation of the free stream conditions in the test section of the HEG free piston driven shock tunnel[17] was based on numerical analysis using a suitable set of measured input parameters. First, the nozzle reservoir temperature was computed with a 1D simulation of the shock tube using ESTC[18]. The relevant input parameters were the measured values of the initial shock tube filling pressure and temperature, the shock speed and the nozzle reservoir pressure. Based on these nozzle reservoir conditions, the free stream was subsequently determined by numerical simulation of the nozzle flow. Different RANS turbulence models were applied to thermal equilibrium

and non-equilibrium computations to determine the influence of different modeling assumptions on the obtained free stream conditions. The computational grid consisting of about 20,000 grid points and the Mach number contours resulting from the thermal non-equilibrium computation are shown in Fig. 1.

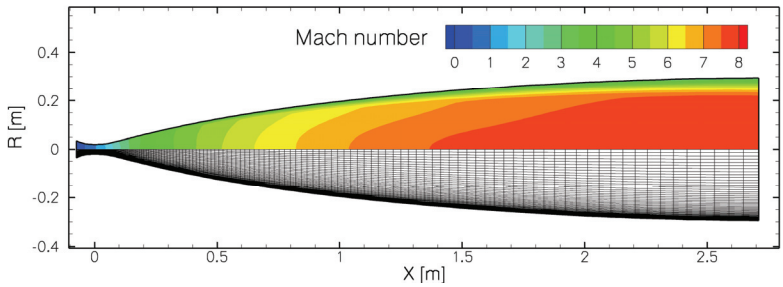

Figure 1: CFD grid and Mach number contours for the HEG nozzle flow (thermal non-equilibrium)

A reservoir-pressure inflow boundary condition is used at the subsonic inflow of the nozzle. The thermodynamic conditions at the inflow are computed using isentropic expansion from prescribed nozzle stagnation conditions using the inflow velocity vector which is part of the CFD solution. The chemical non-equilibrium 5 species and 17 reactions rate set by Gupta[19] is used for this investigation. Previous studies show a good performance of this model for chemical relaxation in high enthalpy wind tunnel nozzles[20]. The considered species are molecular and atomic nitrogen and oxygen (N_2, O_2, N, O) and nitric oxide (NO).

Numerical results for the Pitot pressure profile (Pt2) and the stagnation point heat flux (Qt2) on spherical probes located at the nozzle exit plane in the HEG test section are shown in Fig. 2. The Pitot pressure was computed using the Rayleigh-Pitot equation and the stagnation point heat flux was obtained from a correlation proposed by Verant[21]. The validity of this simplified approach was tested by CFD analysis of the flow past a spherical probe as used in the HEG. It was found that the Rayleigh-Pitot estimation using a ratio of specific heats of 1.4 results in a deviation of 2% from the CFD stagnation pressure and the Verant stagnation point heat flux differs by 5.5% from the CFD.

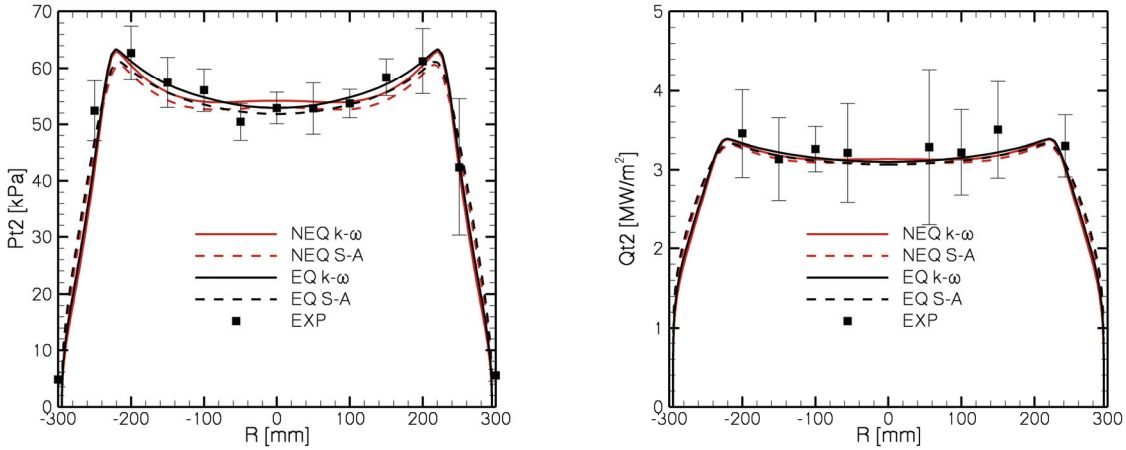

Figure 2: Pitot pressure and stagnation point heat flux for different models to describe the turbulence and thermal relaxation in the nozzle flow. (NEQ: thermal non-equlibrium, EQ: thermal equilibrium, S-A: Spalart-Allmaras turbulence model, k-ω: Wilcox *k-ω* turbulence model, EXP: experiment)

The nozzle supply conditions for the calibration experiment (Fig. 2) were a total pressure of 6.42 MPa and a total temperature of 3000 K resulting in a total enthalpy of 3.7 MJ/kg.

Good agreement is observed between the CFD prediction and the Pitot and heat flux rake measurements. The stagnation heat flux profile in the core flow is independent of the applied turbulence model and the assumption of thermal equilibrium or non-equilibrium. The shape of the Pitot pressure profile changes with the assumption of thermal non-equilibrium. This is due to different ratios of specific heats in the region downstream of the nozzle throat caused by sudden vibrational freezing which changes the local Mach number distribution and therefore the characteristics inside the nozzle. The shape of the boundary layer is predicted to be slightly different between the

Spalart-Allmaras and the Wilcox k-ω turbulence models. The best agreement with the available experimental data was achieved with the application of the Wilcox k-ω turbulence model and the assumption of thermal equilibrium. Nevertheless, all CFD predictions are located within the experimental scatter bars.

The free stream conditions of the HyShot experiment in HEG were recomputed using the actual nozzle supply conditions from the test with the HyShot model installed with a total pressure of 6.75 MPa and a total temperature of 2885 K resulting in a total enthalpy of 3.5 MJ/kg. The Wilcox k-ω model was applied and the conditions were averaged at the nozzle exit plane between the center line and a radius of 200 mm. The resulting free stream conditions are summarized in Table 1.

		thermal equilibrium	thermal nonequlibrium
Mach number		7.20	7.82
Temperature	[K]	294	235
Density	[g/m^3]	10.3	10.7
N_2 mass fraction		0.741	0.741
O_2 mass fraction		0.217	0.217
NO mass fraction		0.041	0.041
O mass fraction		0.001	0.001
N_2 vibrational temperature	[K]	---	2200
O_2 vibrational temperature	[K]	---	1230

Table 1: Averaged free stream conditions obtained by numerical simulation of the nozzle flow for the HEG test with the HyShot model installed.

IV. Intake

The CFD analysis of the HyShot scramjet configuration was split into the planar two dimensional investigation of the intake flow and the three dimensional analysis of the flow inside the combustion chamber. The intake flow was treated separately in order to minimize the computational cost. An overview of the overlapping computational domains and applied boundary conditions of both the 2D intake and the 3D combustion chamber parts is given in Fig.3.

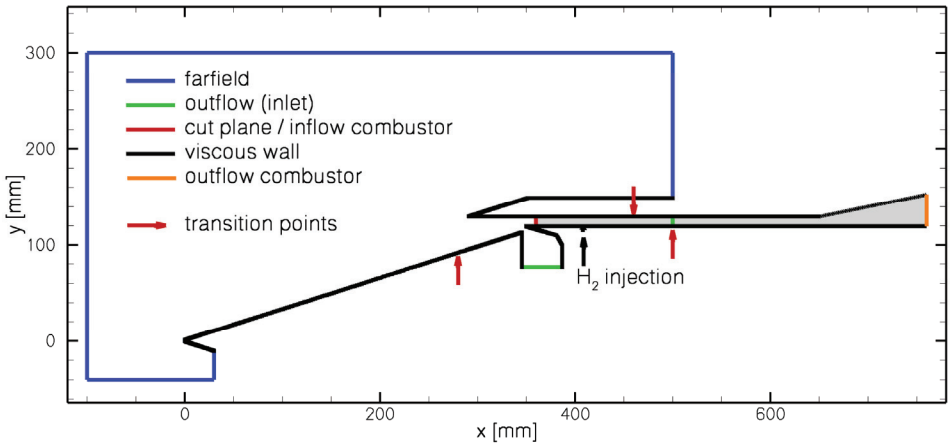

Figure 3: Computational domain and boundary conditions. The three-dimensional domain of the combustion chamber is marked in grey. The locations of transition from laminar to turbulent boundary layers are indicated by the arrows

A detail of the computational grid consisting of about 115,000 grid points in the vicinity of the combustion chamber entrance is shown in the left part of Fig. 4. The unstructured grid was adapted to the resulting shock system. Structured sublayers were used for the resolution of the boundary layers. The flow profile along a cut plane as indicated in Fig. 3 at x = 360 mm downstream of the leading edge is extracted from the 2D intake solution and

then interpolated as a Dirichlet inflow condition to the three dimensional computational grid of the combustion chamber. The averaged inflow conditions from Table 1 were imposed at the farfield boundary. The viscous walls were assumed to be isothermal at a temperature of 300 K and fully catalytic. During the short test time in HEG no significant heating of the walls is expected. The transition from laminar to turbulent flow on the compression ramp was set at x = 280 mm downstream of the leading edge. This transition location corresponds to using a critical Reynolds number of 700,000 which was determined using the measured transition location inside the combustion chamber for fuel-off conditions (see Section V). The reaction rate scheme of Gupta and the Spalart-Allmaras turbulence models were applied.

A detail of the flow field solution assuming thermal equilibrium is shown in the right part of Fig. 4. The Mach number at the entrance of the rectangular combustion chamber duct is about 2.5. A significant part of the compressed flow is spilled outside the cowl. The entire boundary layer is swallowed by the bleed channel as indicated by the streamlines in Fig. 4. No eddy viscosity which is generated inside the transitional boundary layer on the compression ramp, enters the combustion chamber. This supports the validity of the assumption of identical critical Reynolds numbers in the combustor and on the intake ramp.

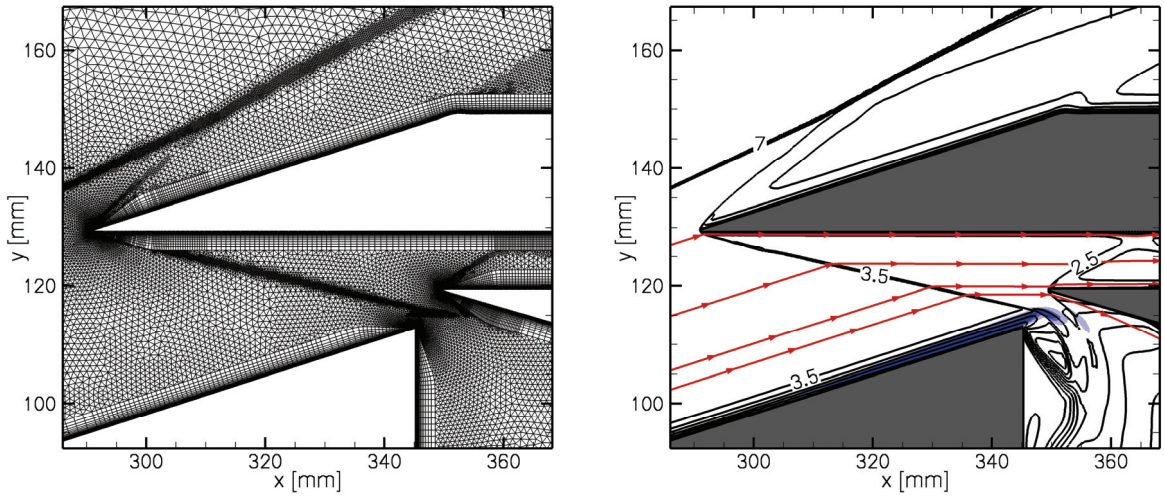

Figure 4: Detail of the CFD grid (left) and detail of the intake flow field. Black: Mach number isolines, red: streamlines and blue: eddy viscosity contours

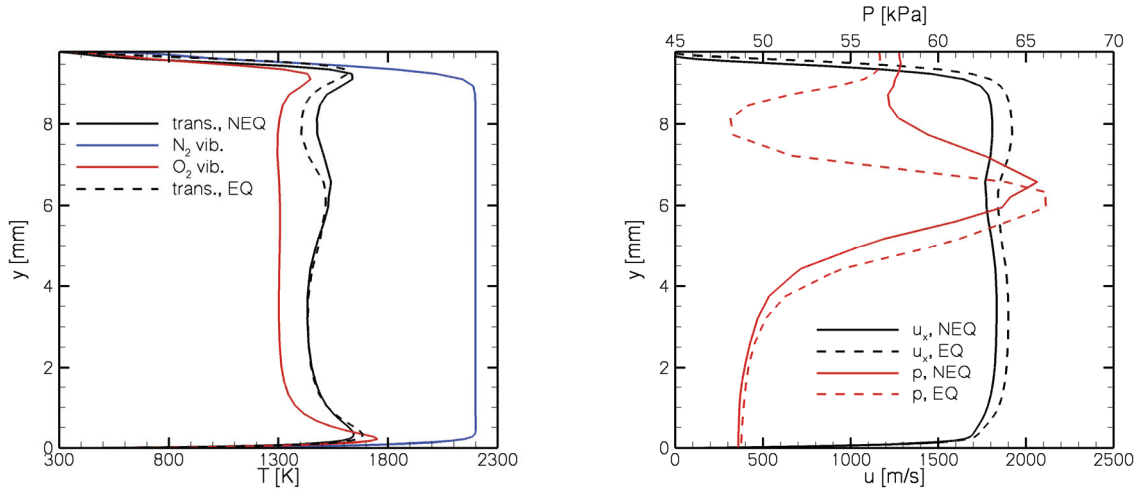

Figure 5: Inflow profiles into the combustion chamber. Left: temperatures, right: pressure and axial velocity. (trans: translational, vib: vibrational, NEQ: thermal non-equilibrium, EQ: thermal equilibrium)

Inflow profiles which are obtained at the cut plane at x = 360 mm are shown in Fig. 5. The application of different turbulence models has no effect on the inflow profiles because the transition location is only 65 mm upstream of the boundary layer bleed and the entire boundary layer is swallowed by the bleed channel. The assumption of thermal non-equilibrium leads to vibrational temperatures which still differ significantly from the translational temperature at the combustor entrance plane. This is due to the rapid exponential growth of vibrational relaxation times especially for the nitrogen molecule at temperatures below 1500 K[14].

The flow velocity at the combustor entrance is slightly higher for the equilibrium flow. The static temperatures are comparable. The variation in the static pressure profiles is caused by the bow shock of the lower combustion chamber lip (see Fig. 4, right). This influence is more pronounced for the flow in thermal equilibrium.

V. Combustion Chamber

The flow field inside the HyShot combustion chamber was simulated using a three dimensional computational domain. The exhaust nozzle was only partially included up to a plane located 110 mm downstream of the end of the rectangular combustion chamber. In order to minimize the computational cost the intake flow is modeled with two dimensional CFD as described in Section IV. Further, all existing symmetries are used. An overview of the computational domain and the applied boundary condition are shown in Fig. 3 and Fig. 6. For better visibility, the plots in Fig. 6, 8, 9 and 10 are shown in a scale of x:y:z of 1:2:2.

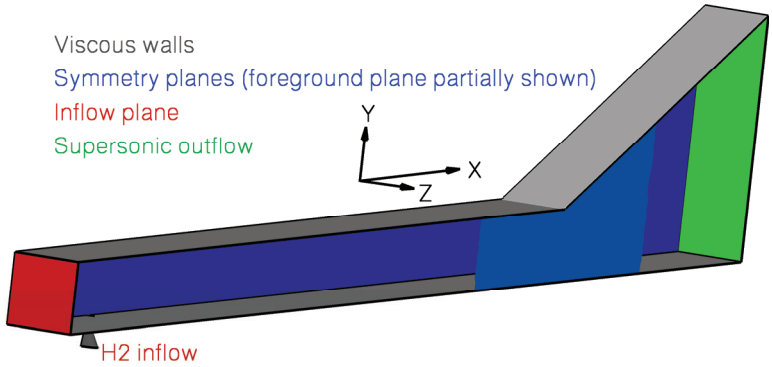

Figure 6: Computational domain and boundary conditions for the combustor

At the inflow plane at an axial location of x = 360 mm downstream of the intake leading edge, the flow profiles obtained from the two dimensional intake analysis are prescribed. The supersonic outflow plane is located at x = 760 mm. The boundary condition which is applied at this plane is a simple extrapolation of the conservative variables which is valid for supersonic flows. The length of the constant cross section part of the combustor ends at x = 650 mm. The height of the combustion chamber in y-direction is 9.8 mm. The width of the HyShot II combustor with four equally spaced porthole injectors is 75 mm. Symmetry boundary conditions are used at the spanwise boundary planes. One is located at z = 0 mm in the center of a porthole injector. The second symmetry plane is located at z = 9.375 mm between two porthole injectors. Therefore, only one eighth of the original spanwise extension of the HyShot configuration is modeled. The influence of the side wall boundary layers is neglected. The bottom wall at y = 0 and the top wall at y = 9.8 mm are modeled with a viscous no-slip boundary condition. Transition from laminar to turbulent flow inside the boundary layers was set at x = 500 mm on the bottom wall and x = 460 mm at the top wall. This transition location was determined by heat flux measurements and corresponds to a critical Reynolds number of 700,000. The wall temperature is fixed to 300 K accounting for the short test times in the HEG facility. The hydrogen injection was modeled by partially including the injector in the computational domain. A reservoir inflow condition as described in Section III was applied at the hydrogen inflow boundary. A total hydrogen pressure of 2.97 bar and a total temperature of 300 K were prescribed. The computational grid which covers this domain consist of 590,000 grid points. Structured prismatic sublayers were used at the viscous wall. A dimensionless wall spacing of y^+ = O(1) was used to ensure sufficient resolution for the low Reynolds number turbulence models and for the computation of the wall heat flux. The grid was successively adapted to density, temperature and total pressure gradients in the flow resulting in an increase of grid points up to 800,000 points. A detail of the computational grid showing the bottom wall and one symmetry plane in the vicinity of the porthole injector is shown in Fig. 7. A modified Jachimowski reaction rate set[15] is applied to the combustor flow. The nine species that are considered are nitrogen (N_2), molecular and atomic oxygen and hydrogen (O_2, O, H_2, H), water

(H_20), hydrogen peroxide (H_2O_2) and the hydroxyl and hydroperoxyl radicals (OH, HO_2). This reaction rate set consist of 17 reactions. The nitrogen chemistry is not considered in this model and N_2 only acts as a passive collision partner. Because of the neglect of nitrogen chemistry, the combustor inflow boundary condition is modified to split the nitric oxide entering the combustor into additional nitrogen and oxygen atoms. The impact of this approximation on the combustion chemistry was not quantified in this study. Nevertheless, the amount of NO entering the combustor is low (mass fraction of 0.041, Table 1).

All simulations of the combustor flow field were performed using the assumption of thermal equilibrium.

Contours of hydrogen mass fraction and streamlines in the $z = 0$ symmetry plane in the vicinity of the porthole injector are shown in Fig. 7. The penetration of the hydrogen jet is about 30% of the total combustor height of 9.8 mm. The vortex system which develops upstream of the injector efficiently enhances the distribution of hydrogen in the boundary layer of the lower combustor wall.

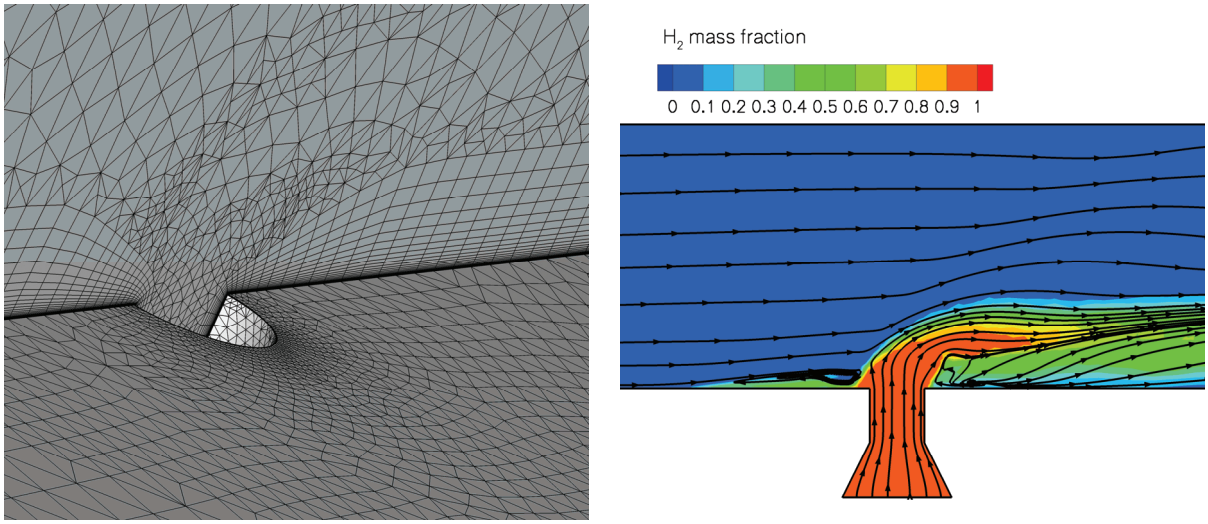

Figure 7: Detail of the computational grid in the vicinity of the hydrogen injection (left), hydrogen mass fraction contours and streamlines in the x-y plane of symmetry through the injector (right)

Representative results for the three dimensional flow field are given in Figures 8 to 10. The cut planes shown in these figures are located at the axial coordinates of x = 450, 500, 550, 600 and 650 mm respectively. The solution which is shown was obtained on the adapted grid with 680,000 grid points and the application of the k-ω turbulence model.

Contours of hydroxyl mass fraction are shown in Fig. 8 together with streamlines emanating from the hydrogen porthole injector. The combustion process starts at the shock which is generated by the injected hydrogen jet. A stabilized supersonic flame develops around the hydrogen flow. The hydrogen which is trapped in the boundary layer starts to react close to the injection location.

Figure 9 shows the contours of static flow temperature. A maximum temperature of 2600 K is reached upstream of the exhaust nozzle. The temperature rise close to the lower combustor wall caused by the consumption of the hydrogen in the boundary layer is clearly visible in the second cut plane.

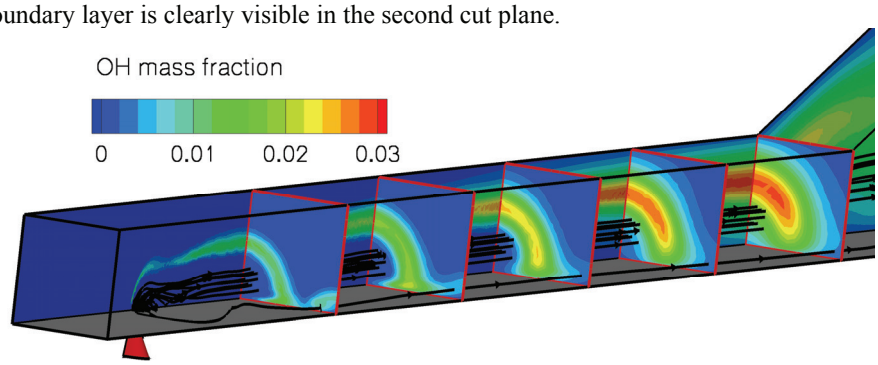

Figure 8: Contours of OH mass fraction and streamlines emanating from the hydrogen injector

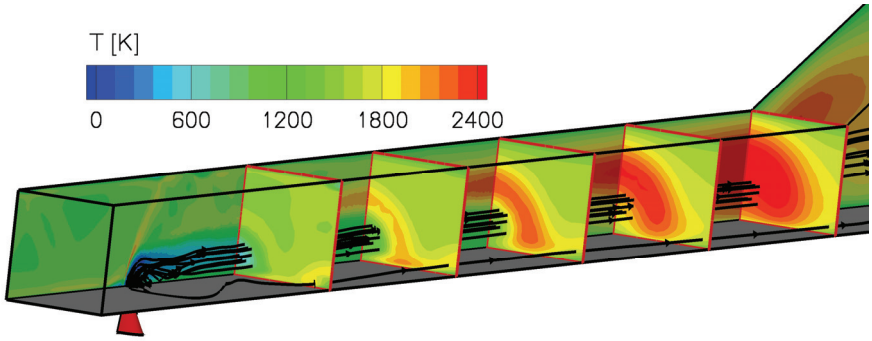

Figure 9: Contours of temperature and streamlines emanating from the hydrogen injector

The Mach number contours are plotted in Fig. 10. The location of the sonic line is also shown in this figure. A small subsonic region develops immediately downstream of the injector. Small separation bubbles are observed at the upper combustor wall upstream of the first cut plane. A large subsonic zone develops further downstream of the combustor. The flow is subsonic over about 10% of the combustor cross sectional area upstream of the exhaust nozzle.

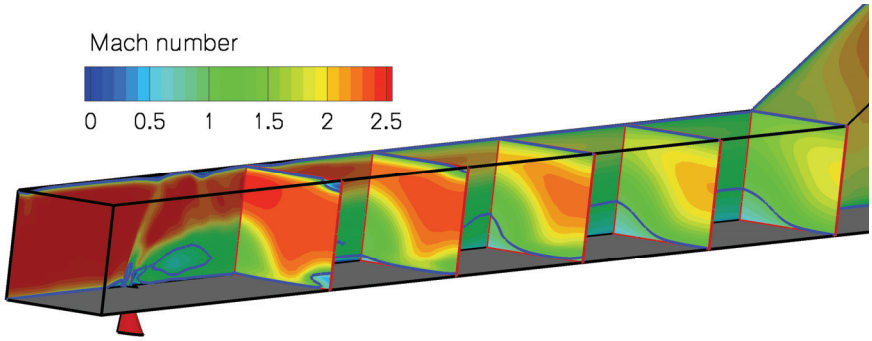

Figure 10: Contours of Mach number. The blue contour line represents sonic velocity.

The pressure distributions on the bottom wall of the combustor along the symmetry line between two injectors are shown in Fig. 11. The square symbols correspond to the associated HEG measurement with an equivalence ratio of $\varphi = 0.43$ at an angle of attack of $\alpha = 3.8$ deg and a Pitot pressure of 61.7 kPa. The scatter bars indicate the RMS values of the measured quantities during the test time. The flight data was taken at an altitude of 33 km, a Pitot pressure of 60 kPa, an angle of attack of $\alpha = 3.6$ deg and a equivalence ratio of $\varphi = 0.30$ which was lower than for the wind tunnel experiment. The fuel-off static surface pressure obtained from CFD analysis (Spalart-Allmaras turbulence model) compares well with the wind tunnel experiment with a slight discrepancy upstream of the axial location of $x = 500$ mm. The reason for this deviation could not be clarified.

Different turbulence models were applied to the fuel-on computations. In the upstream region of the combustor the obtained results are comparable because of the late transition to turbulent boundary layer flow at $x = 500$ mm on the lower combustor wall. In the downstream region of the combustor higher turbulent mixing is predicted by the k-ω model which leads to a higher level of static pressure upstream of the exhaust nozzle compared to the Spalart-Allmaras model. The application of the assumed-PDF approach for the modeling of turbulence-chemistry interactions leads to a further increase of the achieved pressure level but due to the late onset of turbulence this effect remains small. The difference of the peak pressure levels in the combustor which is due to different turbulence modeling assumptions is about 11% (see also Table 2). The influence of the grid density on the pressure distributions was tested by successive adaptation of the grid to density, temperature and total pressure gradients. The results are also presented in Fig. 11. The results on the fine grids show larger variations in the pressure due to better resolved wave structures. Finer grids with less numerical dissipation decrease the fuel mixing and hence the peak pressure level decreases from the base grid to the medium grid by about 4% and to the finest grid by about 6%

The best agreement to the experimental data is achieved by the Wilcox k-ω turbulence model including assumed PDF. The agreement with the flight data is very good, however, it has to be noted that the flight data corresponds to a significantly lower equivalence ratio. The peak pressure level of 135 kPa that was obtained from the HEG experiments was not reached by any of the CFD simulations which underpredicted this value by 10 to 20% (see

Table 2). Further, discrepancies in the qualitative behavior of the pressure distribution between CFD and the HEG experiment are observed. The CFD pressure rises continuously from the injection point at x = 409 mm. The HEG pressures remain at the fuel-off level up to an axial downstream position of about x = 500 mm and then suddenly increase. The clarification of this behavior is the subject of future work.

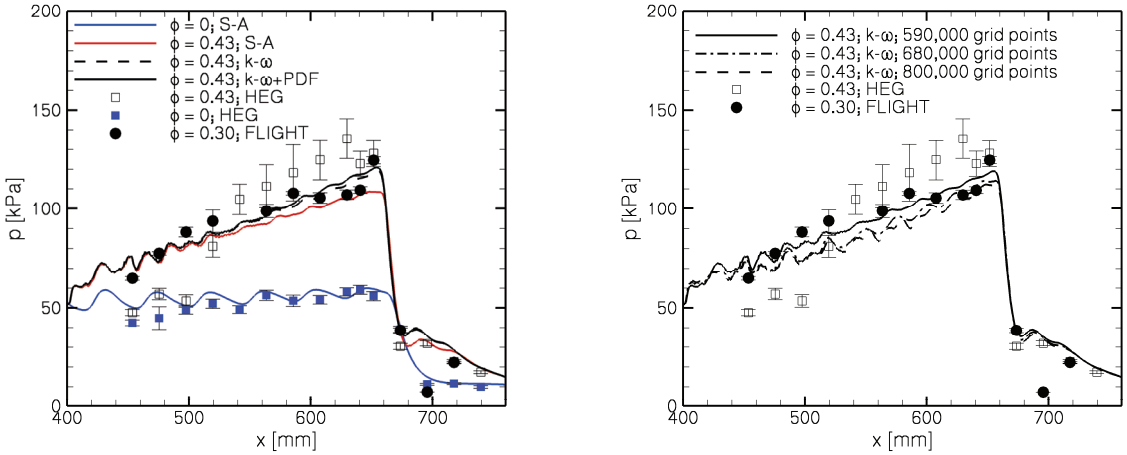

Figure 11: Pressure distribution along the bottom wall of the combustion chamber in the x-y symmetry plane between the hydrogen injectors. (S-A: Spalart-Allmaras turbulence model, k-ω: Wilcox *k-ω* turbulence model, PDF: assumed PDF for turbulence-chemistry interaction)

Surface heat flux distributions on the lower combustor wall downstream of the porthole injector are shown in Fig. 12. Good agreement of the CFD prediction compared to the HEG experiment for both the fuel-on and fuel-off cases is achieved for the application of the Spalart-Allmaras turbulence model. The Wilcox *k-ω* turbulence model significantly overpredicts the measured heat flux levels. The influence of boundary layer transition at x = 500 mm is clearly visible in Fig. 12. An earlier transition at the location of the porthole injection at x = 409 mm leads to a qualitatively different heat flux profile as obtained by the wind tunnel testing. The transition to turbulence, the turbulence modeling, and the heat release due to combustion have a significant impact on the surface heat flux levels.

Integral characteristics of the combustion process for different CFD modeling approaches are summarized in Table 2. The momentum gain, *MG*, is calculated from the differences of total momentum at the inflow and exit planes normal to the flow:

$$MG = \oint\left(\rho u^2 + p\right)dA_{EXIT} - \oint\left(\rho u^2 + p\right)dA_{ENTRANCE} \tag{1}$$

The momentum gain is calculated for the full three dimensional computational domain (FD) including the part to the exhaust nozzle and a reduced domain (RD) which covers only the combustor with constant cross-section up the start of the exhaust nozzle at x = 650 mm. Because the intake is not included in this analysis the figures are not representative for the overall performance. Further it has to be noted that the generic HyShot II scramjet configuration is not designed for net thrust generation. The momentum gain is governed by the skin friction inside of the combustion chamber. Positive values for the full domain result from the effect of expansion inside the nozzle. The values in Table 2 indicate that the application of different turbulence models results in significant differences in the resulting wall shear stresses. The Wilcox *k-ω* models predicts higher momentum losses and shear stresses compared to the Spalart-Allmaras model. This is consistent with the wall heat transfer results. The influence of the grid density and chemistry modeling (PDF) is considerably lower. Further assessment of the performance and applicability of different turbulence models for the prediction of wall heat transfer and shear stresse in reacting supersonic flows is the subject of future work.

A significant amount (between 13 and 20%) of the injected hydrogen remains unburned until the end of the combustion chamber. At the downstream end of the computational domain, these values decrease by about 50% indicating high chemical activity in the upstream region of the exhaust nozzle. The fuel consumption is governed by the mixing process. Despite of the late onset of turbulence, the application of different turbulence models results in substantial differences in the predicted mixing efficiencies and hydrogen consumption rates.

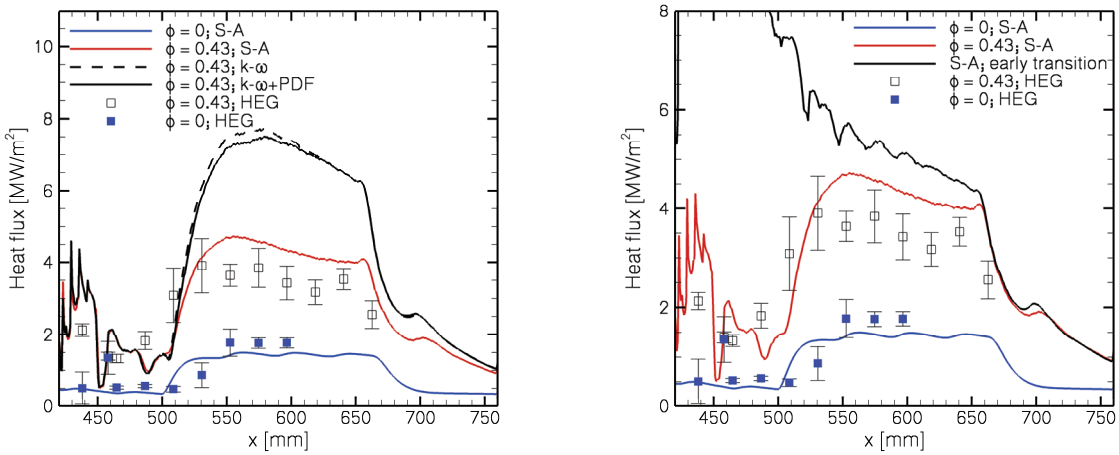

Figure 12: Surface heat flux distribution along the bottom wall of the combustor in the x-y symmetry plane through the hydrogen injector

Case	Max combustor pressure	Momentum gain, RD	Momentum gain, FD	Unburned hydrogen, RD	Unburned Hydrogen, FD
S-A; fuel off	59 kPa	-22.9 N	7.9 N	---	---
S-A	108 kPa	-22.5 N	28.8 N	19.6 %	11.7 %
k-ω	119 kPa	-30.3 N	22.2 N	13.5 %	7.4 %
k-ω, fine grid	114 kPa	-30.3 N	20.4 N	17.5 %	9.1 %
k-ω, finest grid	112 KPa	-29.9 N	19.8 N	20.4 %	10.4 %
k-ω + PDF	121 kPa	-30.3 N	22.4 N	13.3 %	7.3 %

Table 2: Integral characteristics of the combustion process. FD: full domain including exhaust nozzle, RD: reduced domain, only combustion chamber

VI. Summary

The DLR unstructured/hybrid flow solver TAU was extended for the modeling of the flow path in supersonic combustion ramjet engines. Appropriate models for turbulent hydrogen combustion were implemented. This code was applied to determine the free stream conditions in the HEG test section, to simulate the HyShot intake flow field and for the numerical investigation of the turbulent reacting flow in the combustor. The results presented in this paper correspond to the HEG condition XII which duplicates the HyShot free stream conditions at a flight altitude of 32.5 km.

The calculated Pitot pressure and stagnation point heat flux profiles at the exit plane of the wind tunnel nozzle agree well with the experimental results obtained from calibration rake measurements. The boundary layer thickness and profile were correctly predicted by both the Wilcox *k-ω* and the Spalart-Allmaras turbulence models. The numerical analysis of the intake flow field assuming thermal non-equilibrium reveals that the vibrational energy of the nitrogen molecules remains frozen until the entrance plane of the combustion chamber. The quantification of the influence of thermal non-equilibrium on the combustion process itself is subject of future investigations.

The separated and two dimensional treatment of the intake flow decreased the computational cost for the numerical simulation of the HyShot configuration. Additionally, existing symmetries were used to further reduce the three dimensional computational domain of the combustor investigations. The initial penetration of the hydrogen jet emanating from the porthole injection was found to be about 30% of the channel height. The supersonic flow which develops around the injected hydrogen is anchored at the porthole injector. A region of subsonic flow which covers a maximum of about 10% of the total cross sectional area of the combustion chamber develops downstream of the porthole injectors. Satisfactory agreement between CFD and experiment was achieved for the static pressure distribution in the combustor by both turbulence models and for the surface heat flux distribution by the Spalart-

Allmaras model. The CFD analysis confirmed the transition to turbulent boundary layers at 100mm downstream of the injection location.

The numerical analysis of chemically reacting supersonic flows inside scramjet engines is still subjected to uncertainties which are mainly caused by variations in the predictions of the behavior of boundary and mixing layers obtained by the application of different turbulence models. These uncertainties underline the necessity and urgency of precise validation experiments and of a close link between ground testing, CFD analysis and flight experiments.

A new test campaign of the HyShot flight experiment configuration will be carried out in HEG in the near future. These tests will include the application of optical measurement techniques (Schlieren) to the combustor and a considerable increase of the instrumentation density. These tests are expected to provide valuable data for the validation of CFD tools for scramjet applications.

Acknowledgments

This work was performed within the "Long-Term Advanced Propulsion Concepts and Technologies" project investigating high-speed airbreathing propulsion. LAPCAT, coordinated by ESA-ESTEC, is supported by the EU within the 6th Framework Programme Priority 1.4, Aeronautic and Space, Contract no.: AST4-CT-2005-012282. Further info on LAPCAT can be found on http://www.esa.int/techresources/lapcat.

References

[1]Long-Term Advanced Propulsion Concepts and Technologies project investigating high-speed airbreathing propulsion. LAPCAT, coordinated by ESA-ESTEC, is supported by the EU within the *6th Framework Programme* Priority 1.4, Aeronautic and Space, Contract no.: AST4-CT-2005-012282.

[2]Paull, A., Alesi, H., Anderson, S., "The HyShot flight program and how it was developed," *AIAA/AAAF 11th International Space Planes and Hypersonic Systems and Technologies Conference*, Orleans, France, 2002

[3]Gardner, T., Hannemann, K., Paull, A., Steelant, J., "Ground Testing of the HyShot supersonic combustion flight experiment in HEG", *Proceedings of the 24th International Symposium on Shock Waves*, Beijing, 2004

[4] Gerhold, T., Friedrich, O., Evans, J., Galle, M., "Calculation of Complex Three-Dimensional Configurations Employing the DLR-TAU-Code", AIAA-Paper 97-0167, 1997.

[5] Steelant, J., Mack, A., Hannemann, K., Gardner, A. D., "Comparison of Supersonic Combustion Tests with Shock Tunnels, Flight and CFD", *42th AIAA Joint Propulsion Conference and Exhibit, Sacramento (CA)*, 9-12/07 2006

[6]Reimann, B., Johnston, I., Hannemann, V., "The DLR TAU-Code for High Enthalpy Flows," *Notes on Numerical Fluid Mechanics and Multidisciplinary Design*, Vol.87, Springer, 2004

[7]Spalart, P.R., Allmaras, S.R., "A One-Equation Turbulence Model for Aerodynamic Flows," AIAA-Paper 92-0439, 1992

[8]Wilcox, D.C., *Turbulence Modelling for CFD*, DCW Industries, La Canada, California, 1998

[9]Liou, M.S., Edwards, J.R., "AUSM Schemes and Extensions for Low Mach and Multiphase Flows," *30th Computational Fluid Dynamics Lecture Series*, Von Karman Institute for Fluid Dynamics, 1999

[10]Mack, A., Hannemann, V.," Validation of the Unstructured DLR TAU-Code for Hypersonic Flows.", AIAA-Paper 2002-3111, 2002

[11]Wilke, C.R., "A Viscosity Equation for Gas Mixtures," *Journal of Chemical Physics*, Vol. 18(4), 1950

[12]Zipperer, L., Herning, F., „Beitrag zur Berechnung der Zähigkeit technischer Gasgemische aus den Zähigkeitswerten der Einzelbestandteile", *Das Gas- und Wasserfach*, Vol. 4, 1936

[13]Landau, L.D., Teller, E., „Zur Theorie der Schalldispersion (Theory of Sound Dispersion)," *Phys. Z. Sowjetunion*, Vol. 10, No. 34, 1936

[14]Millikan, R. C., White D. R., "Systematics of Vibrational Relaxation", *Journal of Chemical Physics*, Vol. 39, No. 12, 1963, pp 3209-3213

[15]Gerlinger, P., "An Implicit Multigrid Method for Turbulent Combustion", *Journal of Computational Physics*, Vol. 167, 2001, pp. 247-276

[16]Gaffney, R.L., White, J.A., Girimaji, S.S., Drummond, J.P., "Modeling Turbulent Chemistry Interactions using Assumed PDF Methods", *28th AIAA/SAE/ASME/ASEE Joint Propulsion Conference and Exhibit*, 1992

[17]Hannemann, K., Schnieder, M., Reimann, B., Martinez Schramm, J., „The Influence of Driver Gas Contamination in HEG", AIAA-Paper 2000-2593, 2000

[18]McIntosh, M.K., "Computer Program for the Calculation of Frozen and Equilibrium Conditions in Shock Tunnels," *Australian National University*, Canberra A.C.T., 1968

[19]Gupta, R.N., Yos, J.M., Thompson, R.A., Lee, K.P., "A Review of Reaction Rates and Thermodynamic and Transport Properties for an 11-Species Air Model for Chemical and Thermal Nonequilibrium Calculations to 30000 K," *NASA Reference Publication*, No. 1232, 1990

[20]Karl, S., Martinez-Schramm, J., Hannemann, K., "High Enthalpy Cylinder Flow in HEG: A Basis for CFD Validation, " *33rd AIAA Fluid Dynamics Conference*, 2003

[21]Verant, J.L., "Numerical Enthaplies Rebuilding for Perfect Gas and Nonequilibrium Flows. Applications to High-Enthalpy Wind Tunnels", *ONERA-Report*, No. 69/6121 SY, HT-TN-E-1-201-ONER, 1995